



The effect of dioctyl phthalate films on the ammonium nitrate aerosol evaporation rate

Celia N. Cruz, Konstandinos G. Dassios, Spyros N. Pandis*

Carnegie Mellon University, Department of Chemical Engineering, Pittsburgh, PA 15213, USA

Received 24 June 1999; accepted 9 March 2000

Abstract

The evaporation of submicrometer ammonium nitrate (NH_4NO_3) aerosol coated with an organic film was measured in order to determine the effect of the film on mass transfer rate and equilibration time of the semi-volatile inorganic. Ammonium nitrate (NH_4NO_3) particles 100–200 nm in diameter were coated with dioctyl phthalate (DOP) and allowed to evaporate in a constant temperature laminar flow reactor. Evaporation rates for the organic-coated particles were compared to pure ammonium nitrate evaporation at 22 and 27°C. A decrease, up to 50%, in NH_4NO_3 evaporation rate due to the presence of the DOP film was observed. The decrease in evaporation due to the DOP can be described mathematically at 22°C by a decrease in the accommodation coefficient for NH_4NO_3 , $\alpha_{\text{NH}_4\text{NO}_3}$, from 0.4 (the pure NH_4NO_3 value) to 0.25 for the DOP-coated NH_4NO_3 . Similarly, at 27°C, a decrease in $\alpha_{\text{NH}_4\text{NO}_3}$ from 0.3 for the pure NH_4NO_3 to 0.25 for the DOP-coated particles was estimated. The decrease in evaporation rates can also be explained by a decrease in NH_4NO_3 effective diffusivity. The implications to NH_4NO_3 formation and evaporation in the atmosphere are discussed. © 2000 Elsevier Science Ltd. All rights reserved.

Keywords: Atmospheric aerosol; Organic aerosol; Organic films; Equilibrium timescale

1. Introduction

Ammonium nitrate (NH_4NO_3) aerosol is formed from the reaction of gas-phase ammonia and nitric acid and may comprise as much as 30% of the fine aerosol mass (Wexler and Seinfeld, 1990). Under typical atmospheric conditions, NH_4NO_3 is volatile and the equilibrium assumption has been traditionally used to model its concentrations in the atmosphere (Basset and Seinfeld, 1984; Hildemann et al., 1984; Bai et al., 1995). However, this assumption relies on the rapid mass transfer of HNO_3 and NH_3 between the aerosol and the gas phase. Dassios and Pandis (1999) proposed that this assumption is valid for pure submicrometer NH_4NO_3 particles. Their measurements took into account the dependence of NH_4NO_3 evaporation on temperature, relative humid-

ity, gas-phase concentrations, the Kelvin effect, and mass accommodation. However, mass transfer of NH_4NO_3 can be potentially hindered by other factors, such as surface or film effects, which have not been addressed previously. This study focuses on the effect of an organic film on the evaporation rate of NH_4NO_3 aerosol under similar conditions to those measured by Dassios and Pandis (1999).

Typically, organic species represent 25–65% of the fine aerosol mass, where NH_4NO_3 is mostly found (Wolff et al., 1991; Sloane et al., 1991; Chow et al., 1994; Turpin and Huntzicker, 1991; Turpin et al., 1991). Of these species, up to 70% can be secondary organic, particularly during heavy smog episodes. Since secondary organic species are formed from the condensation of low-volatility products of the photooxidation of primary hydrocarbons, the formation of secondary organic films on preexisting atmospheric aerosol is possible (Gill et al., 1983). Organic films could also be formed by primary organic species during the atmospheric processing (e.g. cloud processing, relative humidity cycling, etc.) of a

* Corresponding author.

E-mail address: spyros@andrew.cmu.edu (S.N. Pandis).

particle containing both organic and inorganic components (Gill et al., 1983; Ellison et al., 1999). The effect of organic films has been mostly addressed in studies investigating aerosol water absorption, aqueous droplet evaporation, and cloud condensation nuclei (Andrews and Larson, 1993; Hameri et al., 1992; Shulman et al., 1997; Xiong et al., 1998; Cruz and Pandis, 1998). However, little is known about the effect of organic films on the evaporation of semi-volatile inorganic aerosol such as NH_4NO_3 .

In this study the evaporation of NH_4NO_3 aerosol coated with dioctyl phthalate (DOP) is measured at 22 and 27°C. The results are compared to pure NH_4NO_3 aerosol evaporation and to the theory developed by Dassios and Pandis (1999). DOP was chosen as the surrogate organic to model organic films that might hinder the mass transport of the inorganic core species during evaporation. This compound was chosen due to its hydrophobicity, high molecular weight, propensity to form uniform films, and other properties that make it a good model for organic film studies (Ziemann and McMurry, 1998; Liang et al., 1997; Cruz and Pandis, 1998). DOP is condensed on the NH_4NO_3 aerosol and the coated particles are allowed to evaporate in a temperature-controlled laminar flow reactor. The coating process and evaporation measurements are described below.

2. Experimental

The experimental setup used in this study is shown in Fig. 1. The main components include the particle generation system, the organic coating system, the constant temperature laminar flow reactor, and the particle sizing system. The function of these components is described below. The tandem differential mobility analyzer (TDMA) setup and laminar flow reactor used to measure NH_4NO_3 evaporation are described in detail in Dassios and Pandis (1999). The latest addition to the system consists of a particle coating system as described in Cruz and Pandis (1998).

2.1. Particle generation

The NH_4NO_3 particles are formed from the atomization (constant output atomizer 3076; TSI, Inc.) of a double de-ionized water- NH_4NO_3 solution (1 wt%) fed by a syringe pump. The aerosol is then dried in the diffusion dryer at $\text{RH} < 6\%$. This low relative humidity is maintained throughout the experimental system. The dry NH_4NO_3 particles then enter the neutralizer where they are exposed to a Kr-85 bipolar source and are allowed to reach a nearly Boltzmann distribution of charges. The dry charged NH_4NO_3 aerosol then enters

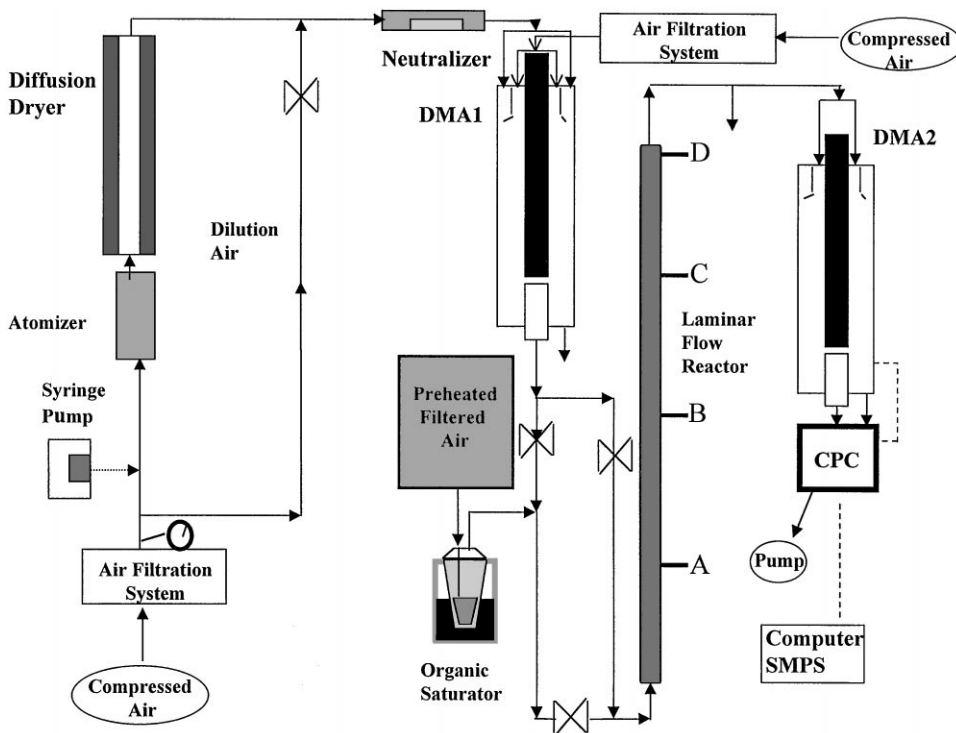


Fig. 1. TDMA experimental setup.

the first differential mobility analyzer (DMA1; electrostatic classifier 3071A, TSI Inc.) where a nearly monodisperse distribution of particles is generated by selecting the corresponding voltage for the desired peak diameter. The initial diameters used in these experiments were 100, 120, 140, 180, and 200 nm. This diameter range allows flexibility for observing evaporation for a greater range of temperatures, given that NH_4NO_3 particles of these sizes will not evaporate completely for $T < 30^\circ\text{C}$ during the residence time of interest (Dassios and Pandis, 1999). The monodisperse NH_4NO_3 aerosol distribution can either bypass or enter the organic coating system depending on whether pure or coated NH_4NO_3 evaporation is being measured. If the NH_4NO_3 particles are coated with DOP, $(\text{NH}_4)_2\text{SO}_4$ aerosol must be used to measure the thickness of the organic film during condensation because it does not evaporate as is the case with NH_4NO_3 . This procedure is described in the following sections.

2.2. Organic film coating

Filtered dry air is allowed to pass through a stainless-steel heating coil ($T_{\text{air}} > 50^\circ\text{C}$) and then through the glass saturator containing the desired organic for coating. In the case of this experiment, the coating organic is DOP. The saturator bottle filled with DOP is kept in a constant temperature water bath at $T = 90^\circ\text{C}$. The organic-saturated air is then mixed with the monodisperse NH_4NO_3 aerosol exiting DMA1 and the mixture is then allowed to enter the laminar flow reactor. The organic film thickness depends on the mixing ratio of organic-saturated air to aerosol flow rate and can be varied by changing these flows. Fig. 2 shows the organic

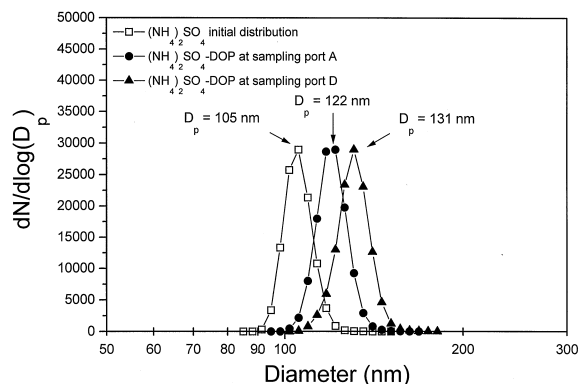


Fig. 2. Sample $(\text{NH}_4)_2\text{SO}_4$ size distributions as measured by SMPS before and after condensation of DOP. The initial uncoated distribution shown has a peak diameter of 105 nm, while the DOP-coated distributions have a film thickness of 9 nm at reactor sampling port A and a film thickness of 13 nm at sampling port D.

film coating results for a representative experiment. A film of roughly 10 nm thickness is created by the time the particles reach point A in the reactor, while at point D the film has grown an additional 4 nm. Once the organic film thickness is set by controlling the individual flowrates, the final distribution shows a variability of less than 5% in final particle diameter and of less than 10% in total number concentration during each experiment, which indicates that the system is stable. Using the amount of DOP condensed on the particles one can estimate the vapor pressure of DOP in the gas phase during the coating stage to be of the order of 10^{-5} Pa. This is of the same order of magnitude as the concentrations of semi-volatile organic compounds in the atmosphere (Seinfeld and Pandis, 1998).

2.3. Constant temperature laminar flow reactor

The laminar flow reactor is a 2.54 cm i.d. SS tube of 4 m in length. The reactor is kept at constant temperature by a heating/cooling water jacket, which is controlled by a constant temperature water bath. There are four sampling ports on the reactor, which are located at 1 m intervals from the inlet. The sampling ports are labeled as A (1 m), B (2 m), C (3 m), and D (4 m) (Fig. 1). These sampling ports allow for variation in reactor residence time and intermediate measurements of particle size change during the evaporation experiments. The temperature control system allows only a $\pm 0.1^\circ\text{C}$ variance in temperature as observed from measurements along the five sampling ports, thus validating the assumption of isothermal conditions during evaporation (Dassios and Pandis, 1999).

2.4. Particle sizing

The particle sizing system consists of DMA2 and the condensation particle counter (CPC, 3010 TSI, Inc.; scanning mobility particle sizing system (SMPS) 3934 TSI, Inc.). The particle distributions can be measured at any of the reactor sampling ports as well as before and after the reactor. Total distribution sampling times can be between 1 and 6 min. Accurate and repeatable results were observed with sampling times of 3 min.

2.5. Procedure

The main goal of this study is to determine the effect of an organic film on NH_4NO_3 evaporation. Given that condensation of the organic film and evaporation of NH_4NO_3 occur simultaneously within the reactor, one needs to determine which portion of the change in size is due to evaporation of the inorganic core and which is due to condensation of the organic film. To decouple these two processes, a control experiment using a non-volatile inorganic core (e.g. $(\text{NH}_4)_2\text{SO}_4$) is performed to determine the mass change due to the organic film

condensation. A monodisperse distribution of $(\text{NH}_4)_2\text{SO}_4$ is used to measure the amount of organic mass deposited on the particles due to condensation of the organic film. Fig. 3 illustrates the changes in diameter that occur for $(\text{NH}_4)_2\text{SO}_4$ and NH_4NO_3 particles during coating/evaporation. The $(\text{NH}_4)_2\text{SO}_4$ particles continue to grow due to DOP condensation until they reach equilibrium between sampling ports A and B. The NH_4NO_3 particles, however, evaporate as well as grow due to DOP condensation, resulting in a net loss of NH_4NO_3 mass (Fig. 3). The DOP volume gained due to condensation of the film can be determined from the $(\text{NH}_4)_2\text{SO}_4$ experiments. As a first-order approximation, because of the small difference in size between the NH_4NO_3 and $(\text{NH}_4)_2\text{SO}_4$ particles, we assume that the same mass condensed on both particles. Also, this experiment assumes that DOP shows no preference for condensing on $(\text{NH}_4)_2\text{SO}_4$ or NH_4NO_3 , thus condensing equally on both substrates. This assumption is consistent with the results of Cruz and Pandis (1999), who did not observe any preference for the condensation of DOP on a number of different inorganic and organic aerosol particles under similar conditions. Thus, the DOP volume is subtracted from the NH_4NO_3 /DOP particle volume in order to calculate the real NH_4NO_3 volume change due to evaporation. Evaporation rates for NH_4NO_3 are determined for the last 3 m of the reactor, between sampling ports A and D, in order to minimize the effects of simultaneous condensation and evaporation during an experiment. Sampling port A is chosen over port B as the initial point, in order to maximize residence time and increase

the likelihood of measuring significant changes in diameter due to evaporation.

The mass of NH_4NO_3 evaporated between sampling ports A and D, $\Delta M_{\text{NH}_4\text{NO}_3}$, is determined from

$$\Delta M_{\text{NH}_4\text{NO}_3} = (V_{\text{NH}_4\text{NO}_3\text{A}} - V_{\text{NH}_4\text{NO}_3\text{D}})\rho_{\text{NH}_4\text{NO}_3}, \quad (1)$$

where $V_{\text{NH}_4\text{NO}_3\text{A}}$ and $V_{\text{NH}_4\text{NO}_3\text{D}}$ are the volumes of NH_4NO_3 in the particle at sampling ports A and D, respectively, and $\rho_{\text{NH}_4\text{NO}_3}$ is the density of NH_4NO_3 . In order to calculate the values for $V_{\text{NH}_4\text{NO}_3\text{A}}$ and $V_{\text{NH}_4\text{NO}_3\text{D}}$ for the coated particles, a complete series of measurements for a full experiment at a given temperature and residence time consists of the following steps:

1. *Measurement of size of the $(\text{NH}_4)_2\text{SO}_4$ particles coated with DOP at sampling port A.* The measurements are performed at the 1 m sampling port to quantify the amount of DOP condensation between DMA1 and the sampling port A, V_{DOP_A} :

$$V_{\text{DOP}_A} = \frac{1}{6}\pi D_{\text{p}(\text{NH}_4)_2\text{SO}_4 - \text{DOP}_A}^3 - \frac{1}{6}\pi D_{\text{p}(\text{NH}_4)_2\text{SO}_4\text{initial}}^3. \quad (2)$$

Eq. (2) describes how the final diameters measured at port A, $D_{\text{p}(\text{NH}_4)_2\text{SO}_4 - \text{DOP}_A}$, are used to calculate V_{DOP_A} . This measurement with $(\text{NH}_4)_2\text{SO}_4$ is performed once the coating system and reactor temperatures are stable. Also, V_{DOP_A} will be used to calculate the initial amount of NH_4NO_3 in the particles at port A.

2. *Measurement of size of the NH_4NO_3 particles coated with DOP at sampling port A.* The measurements for the same initial particle diameters are repeated for NH_4NO_3 particles at the 1 m sampling port, in order to measure the corresponding diameter for the NH_4NO_3 -DOP particles, $D_{\text{pNH}_4\text{NO}_3 - \text{DOP}_A}$:

$$V_{\text{NH}_4\text{NO}_3\text{A}} = \frac{1}{6}\pi D_{\text{pNH}_4\text{NO}_3 - \text{DOP}_A}^3 - V_{\text{DOP}_A}. \quad (3)$$

This is done to correct for evaporation of NH_4NO_3 between DMA1 and sampling port A, in order to calculate the initial mass of NH_4NO_3 for evaporation between sampling ports A and D (Eq. (3)).

3. *Measurement of size of the $(\text{NH}_4)_2\text{SO}_4$ particles coated with DOP at sampling port D.* The final $(\text{NH}_4)_2\text{SO}_4$ diameters after DOP condensation are used to determine the volume change, V_{DOP_D} , by the time they reach the reactor outlet (Eq. (4)). From this value, it is possible to determine how much DOP has condensed on the particles between sampling ports A and D ($V_{\text{DOP}_D} - V_{\text{DOP}_A}$), which may be used to derive complete condensation rate profiles for the system if necessary:

$$V_{\text{DOP}_D} = \frac{1}{6}\pi D_{\text{p}(\text{NH}_4)_2\text{SO}_4 - \text{DOP}_D}^3 - \frac{1}{6}\pi D_{\text{p}(\text{NH}_4)_2\text{SO}_4\text{initial}}^3. \quad (4)$$

4. *Measurement of size of the NH_4NO_3 particles coated with DOP at sampling port D.* The measurements for

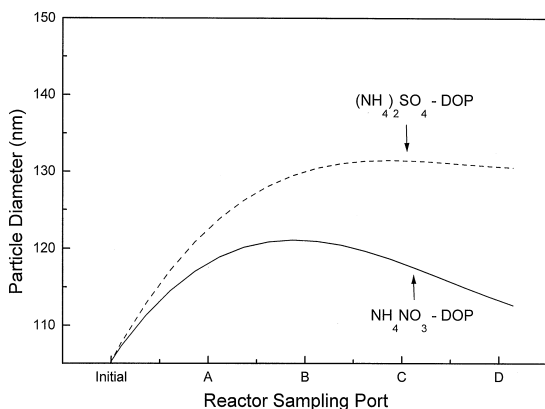


Fig. 3. Measured peak diameters for $(\text{NH}_4)_2\text{SO}_4$ and NH_4NO_3 along the reactor during a typical experimental run. The $(\text{NH}_4)_2\text{SO}_4$ particles grow due to DOP condensation, which occurs primarily in the first third of the reactor volume. This profile is used to calculate the amount of DOP condensed on the NH_4NO_3 distribution. The NH_4NO_3 particles are shown to grow due to DOP condensation and shrink due to NH_4NO_3 evaporation, thus having a smaller final diameter.

the same initial particle diameters above are repeated for NH_4NO_3 in order to measure the corresponding final diameter for the NH_4NO_3 -DOP particles, $D_{p\text{NH}_4\text{NO}_3 - \text{DOP}}$. This final diameter is then used to calculate the final volume of the NH_4NO_3 core after evaporation by

$$V_{\text{NH}_4\text{NO}_3\text{D}} = \frac{1}{6}\pi D_{\text{pNH}_4\text{NO}_3 - \text{DOP}}^3 - V_{\text{DOPD}} \quad (5)$$

Therefore, by measuring final diameters for the coated $(\text{NH}_4)_2\text{SO}_4$ and NH_4NO_3 particles at two points in the reactor, $V_{\text{NH}_4\text{NO}_3\text{a}}$ and $V_{\text{NH}_4\text{NO}_3\text{D}}$ can be calculated and a $\Delta M_{\text{NH}_4\text{NO}_3}$ value can be obtained. The above procedure was repeated for NH_4NO_3 and $(\text{NH}_4)_2\text{SO}_4$ initial particle diameters ranging from 100 to 200 nm at 22 and 27°C. The residence time for evaporation is determined by the flowrate through the reactor and was set to be 21 s for all coated measurements.

3. Theory

The theoretical expression which describes the evaporation rate of an NH_4NO_3 particle is (Dassios and Pandis, 1999)

$$\frac{dD_p}{dt} = 2 \frac{W}{W_0} \frac{[\beta - \sqrt{\gamma + 4D_{\text{HNO}_3} D_{\text{NH}_3} F(\text{Kn}_{\text{HNO}_3}) F(\text{Kn}_{\text{NH}_3}) K(T, H) \exp(a)}]}{\rho D_p} M W_{\text{NH}_4\text{NO}_3},$$

$$a = \frac{4\sigma v}{RTD_p},$$

$$\beta = D_{\text{HNO}_3} C_{\text{HNO}_3}^\infty F(\text{Kn}_{\text{HNO}_3}) + D_{\text{NH}_3} C_{\text{NH}_3}^\infty F(\text{Kn}_{\text{NH}_3}),$$

$$\gamma = [D_{\text{HNO}_3} C_{\text{HNO}_3}^\infty F(\text{Kn}_{\text{HNO}_3}) - D_{\text{NH}_3} C_{\text{NH}_3}^\infty F(\text{Kn}_{\text{NH}_3})]^2, \quad (6)$$

where D_p is the NH_4NO_3 particle diameter, W is the wet mass of the particle at a given relative humidity, W_0 is the dry particle mass, D_i is the diffusivity of species i , $K(T, RH)$ is the equilibrium constant for NH_4NO_3 (Mozurkewich, 1993; Ansari and Pandis, 1999), C_i^∞ is the bulk gas-phase concentration of i , ρ is the particle density, σ is the particle surface tension, v is the particle molecular volume, and R is the gas constant. The corrections for transition regime mass transfer by Fuchs and Sutugin (1971) are also incorporated in the theory as

$$F(\text{Kn}_i) = \frac{1 + \text{Kn}_i}{1 + 0.3773\text{Kn}_i + 1.33\text{Kn}_i(1 + \text{Kn}_i)/\alpha_i}, \quad (7)$$

$$\text{Kn}_i = \frac{2\lambda_i}{D_p}.$$

This expression contains the Knudsen number for the particle, Kn_i , as well as the mean free path, λ_i , and the accommodation coefficient, α_i , for the evaporating species. The $\alpha_{\text{NH}_4\text{NO}_3}$ is defined as the probability that an evaporating molecule of NH_4NO_3 will leave the particle surface instead of returning to the surface. In effect, it

is a parameter that describes the kinetic limitations to mass transfer. Dassios and Pandis (1999) measured $\alpha_{\text{NH}_4\text{NO}_3}$ values for the evaporation of pure NH_4NO_3 ranging from 0.8 to 0.5 ± 0.2 as temperature increases from 20 to 27°C. In this study, the theory presented above is used to analyze the coated NH_4NO_3 evaporation experiments in order to determine any change in evaporation efficiency due to the presence of the organic film.

4. Results

The results for the evaporation of pure and DOP-coated NH_4NO_3 at 27°C are presented in Fig. 4. The average DOP film thickness for the experiments at 27°C was 14 ± 3 nm, and was maintained constant with size. At this temperature, the fraction of NH_4NO_3 that evaporates for the pure experiment decreases from 0.72 to 0.42 with increasing particle diameter between 100 and 200 nm (Fig. 4). In the case of the DOP-coated particles, the mass loss upon evaporation drops more sharply with size, from 0.84 to 0.22 for the same range of sizes. This

trend was also observed at 22°C, where the NH_4NO_3 mass loss upon evaporation decreases from 0.56 to 0.32 for the pure particles and from 0.62 to 0.23 for the DOP-coated particles with increasing initial NH_4NO_3 diameter. The measurements at 22°C had an average DOP film thickness of 10 ± 2 nm. In general, the fraction of NH_4NO_3 mass lost due to evaporation is decreased by the presence of the DOP film. The DOP coating effect on the NH_4NO_3 mass loss appears to be dependent on size. That is, the DOP is more efficient in decreasing the evaporation rate for the larger particles (> 150 nm). Since the DOP film thickness was maintained constant with particle size, this alone cannot explain the observed size dependence of the reduction in NH_4NO_3 evaporation.

In an attempt to quantify the observed effect of the DOP film, the mass transfer theory presented in the preceding section can be used (Eqs. (6) and (7)). Given that the pure and DOP-coated experiments were conducted under the same conditions in terms of temperature,

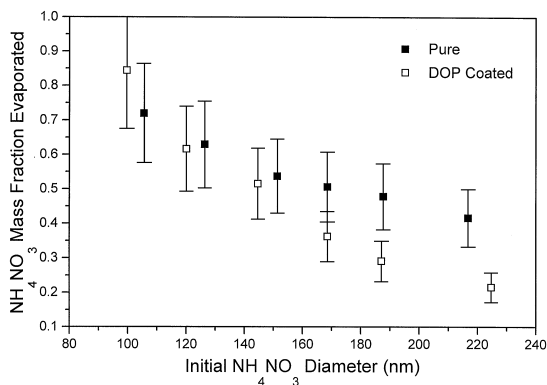


Fig. 4. Measured fraction of NH_4NO_3 mass lost due to evaporation, $\Delta M_{\text{NH}_4\text{NO}_3}/M_{\text{NH}_4\text{NO}_3\text{initial}}$, versus initial NH_4NO_3 peak diameter. Results are shown for pure and DOP-coated NH_4NO_3 particles at 27°C and a residence time of 21 s. The error bars indicate the uncertainty in $\Delta M_{\text{NH}_4\text{NO}_3}$, as calculated from the measured diameters.

relative humidity, residence time, and concentrations, the first parameter to address is the accommodation coefficient for NH_4NO_3 . The theory does not explicitly account for the additional mass transfer resistance presented by the organic film. Neglecting the film thickness for the time being, the effect can be approximated as a surface change and modeled with the same accommodation coefficients. For the analysis, the final and initial $V_{\text{NH}_4\text{NO}_3}$ values measured from Eqs. (3) and (5) were converted to NH_4NO_3 particle diameters before and after evaporation. Using Eqs. (6) and (7) the $\alpha_{\text{NH}_4\text{NO}_3}$ values necessary to model the NH_4NO_3 evaporation observed experimentally can be calculated for the initial and final diameters. The results are presented in Figs. 5 and 6 for the two experimental temperatures. At 22°C , the average $\alpha_{\text{NH}_4\text{NO}_3}$ for pure NH_4NO_3 evaporation is 0.4 while the DOP-coated NH_4NO_3 evaporation is best described by an average $\alpha_{\text{NH}_4\text{NO}_3}$ of 0.25 (Fig. 5). The differences in evaporation between the coated and pure NH_4NO_3 particles were statistically significant at the 95% confidence interval for particles larger than 120 nm. Similarly, at 27°C , a decrease in $\alpha_{\text{NH}_4\text{NO}_3}$ from 0.3 for the pure experiment to 0.25 is observed for the DOP-coated experiments (Fig. 6). Even though the decrease in average $\alpha_{\text{NH}_4\text{NO}_3}$ due the DOP seems less evident at 27°C , the dependence in diameter is more observable and $\alpha_{\text{NH}_4\text{NO}_3}$ values as low as 0.16 are observed. Dassios and Pandis (1999) reported $\alpha_{\text{NH}_4\text{NO}_3}$ values of 0.8 ± 0.2 and 0.5 ± 0.2 for pure NH_4NO_3 evaporation at 20 and 27°C , respectively. This indicates that our pure NH_4NO_3 evaporation measurements are in general agreement with previous observations and that the coated evaporation results are explained by an $\alpha_{\text{NH}_4\text{NO}_3}$ value which is lower than those measured for the pure NH_4NO_3 in both studies. The observed dependance of

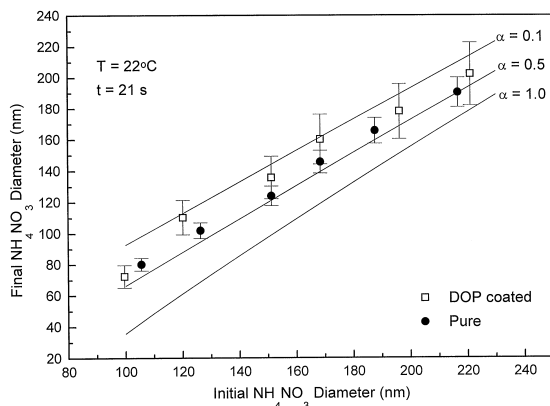


Fig. 5. Experimental results for NH_4NO_3 evaporation at 22°C . The hollow squares represent the DOP-coated NH_4NO_3 evaporation experiments that are compared to the pure NH_4NO_3 evaporation (solid circles). The solid lines represent theoretical predictions for evaporation using different values of $\alpha_{\text{NH}_4\text{NO}_3}$. The error bars indicate the uncertainty in measured final diameters for the pure NH_4NO_3 experiment and the uncertainty in calculated final diameter for the coated NH_4NO_3 particles.

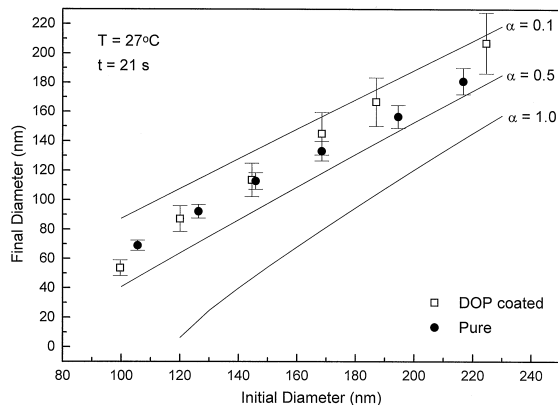


Fig. 6. Experimental results for NH_4NO_3 evaporation at 27°C . The hollow squares represent the DOP-coated NH_4NO_3 evaporation experiments that are compared to the pure NH_4NO_3 evaporation (solid circles). The solid lines represent theoretical predictions for evaporation using different values of $\alpha_{\text{NH}_4\text{NO}_3}$. The error bars indicate the uncertainty in measured final diameters for the pure NH_4NO_3 experiment and the uncertainty in calculated final diameter for the coated NH_4NO_3 particles.

$\alpha_{\text{NH}_4\text{NO}_3}$ on size, which was also observed by Dassios and Pandis (1999) is not easily explained by any available theory.

4.1. Sensitivity analysis

The overall decrease in NH_4NO_3 evaporation is modeled by the theoretical framework presented as an

increased kinetic limitation to mass transfer due to the presence of the DOP film. Dassios and Pandis (1999) conducted a sensitivity analysis in order to confidently conclude that the deviation from perfect evaporation ($\alpha_{\text{NH}_4\text{NO}_3} = 1.0$) in the pure NH_4NO_3 experiments was real and not due to experimental error. The analysis included looking at variations in temperature, surface tension, diffusivity, and liquid water content in the particle. Overall, they concluded that the observed $\alpha_{\text{NH}_4\text{NO}_3}$ values were different from 1.0 and that other uncertainties in the system could not account for the NH_4NO_3 evaporation rates observed. This exercise can be repeated for the coated experiments in order to assess the contribution of these parameters to the observed reduction in NH_4NO_3 evaporation. Given that the temperature variations and the relative humidity (RH < 10%) in our study were the same as observed in Dassios and Pandis (1999), these were not considered to be contributors to the measured decrease in NH_4NO_3 evaporation.

In order to examine the apparent size dependence of the effect of the DOP film on NH_4NO_3 evaporation, one can look at parameters that affect mass transfer and have a more direct effect on particle size. An example of such a parameter is the surface tension, σ , of the particle, because it controls the Kelvin effect which is size dependent. The value for σ used in the previous calculations is 120 erg cm^{-2} (0.12 J m^{-2}). This value was chosen by Dassios and Pandis (1999) from a series of extrapolated values available for NH_4NO_3 (Stelson and Seinfeld, 1982; Mozurkewich, 1993; Wexler and Seinfeld, 1990). The evaporation of NH_4NO_3 was recalculated using a different value for the particle surface tension and for the accommodation coefficient values relevant to this study. Even in the extreme scenario that the DOP film decreases the surface tension of the particle from that of pure NH_4NO_3 to that of pure DOP (33 erg cm^{-2}) (Tao and McMurry, 1989), there is no detectable effect on the final diameter after evaporation. For example, a 200 nm NH_4NO_3 particle which is predicted to evaporate to a final diameter of 152.6 nm after 21 s will actually evaporate to 153.5 nm assuming a lower surface tension (assuming $T = 27^\circ\text{C}$, $\alpha_{\text{NH}_4\text{NO}_3} = 0.5$). Also, there was no

observable size dependence on the amount of NH_4NO_3 evaporated from the particles assuming a lower surface tension, beyond that which is normally observed in the base case. For example, under the same conditions of the previous case, a 100 nm NH_4NO_3 particle would be predicted to evaporate to 40.7 nm assuming $\sigma = 120 \text{ erg cm}^{-2}$ and to 43.7 nm if $\sigma = 33 \text{ erg cm}^{-2}$. In other words, a change in surface tension size due to the presence of the DOP does not capture the secondary dependence of evaporation on initial particle size which was observed in our experiments (Figs. 5 and 6). Therefore, the Kelvin effect alone cannot explain the decrease in evaporation observed due to the DOP coating.

A size-dependant effective diffusivity for NH_3 and HNO_3 , D_{eff} , can be estimated which would model the NH_4NO_3 evaporation rates observed in the presence of the DOP film. The D_{eff} values quantify the net diffusion of NH_3 and HNO_3 through the DOP film as well as into the gas phase. These values were calculated by varying D_{HNO_3} and D_{NH_3} in Eq. (6) until achieving the evaporation rates observed experimentally. In all cases, D_{HNO_3} and D_{NH_3} are assumed to be equal. Table 1 is a summary of the D_{eff} values necessary to reproduce the evaporation rates observed for the DOP-coated NH_4NO_3 at 22 and 27°C . The D_{eff} values are calculated for two assumptions of $\alpha_{\text{NH}_4\text{NO}_3}$, 0.4 and 0.3, which correspond to the values measured for pure NH_4NO_3 evaporation at 22 and 27°C , respectively. No value is shown for the 99.6 nm NH_4NO_3 particle at 27°C , because the particle could not reach the final diameter observed experimentally in the given residence time (21 s) with a lower diffusivity. The average D_{eff} values calculated were 0.046 and $0.047 \text{ cm}^2 \text{ s}^{-1}$ for 22 and 27°C , respectively (Table 1). They can be compared with the values for D_{HNO_3} and D_{NH_3} in Eq. (6) which have been traditionally used in models for pure NH_4NO_3 evaporation ($0.11 \text{ cm}^2 \text{ s}^{-1}$) (Dassios and Pandis, 1999; Wexler and Seinfeld, 1992). This comparison indicates that the DOP coating results in a decrease in NH_4NO_3 diffusivity from the particle by an average factor of 2.4. Given that the film thickness was constant with size during the experiments, quantifying the observed decrease in NH_4NO_3

Table 1
Effective diffusivity for DOP-coated NH_4NO_3 particle evaporation^a

Initial diameter (nm)	D_{eff} ($\text{cm}^2 \text{ s}^{-1}$), $T = 27^\circ\text{C}$, $\alpha_{\text{NH}_4\text{NO}_3} = 0.3$	Initial diameter (nm)	D_{eff} ($\text{cm}^2 \text{ s}^{-1}$), $T = 22^\circ\text{C}$, $\alpha_{\text{NH}_4\text{NO}_3} = 0.4$
100	—	100	0.10
120	0.070	120	0.011
145	0.070	151	0.030
169	0.036	169	0.012
187	0.031	196	0.055
225	0.029	221	0.065

^aDOP film thickness is 14 ± 3 nm for 27°C and 10 ± 2 nm for 22°C experiments. This is not included in the initial diameter value.

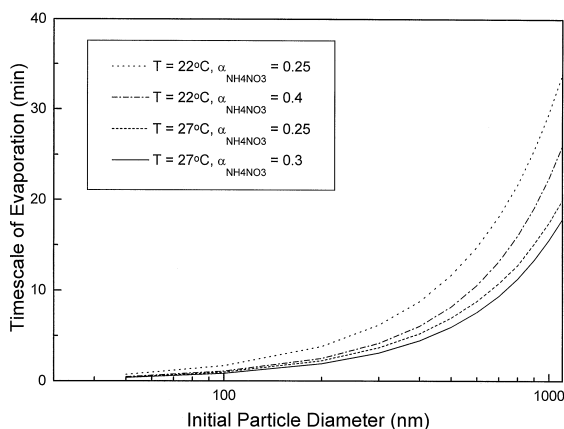


Fig. 7. Predicted timescales of NH_4NO_3 evaporation versus initial particle diameter assuming the reduced $\alpha_{\text{NH}_4\text{NO}_3}$ measured for the DOP-coated NH_4NO_3 particles. Results for 22 and 27°C are shown.

evaporation as a decrease in overall diffusivity indicates that NH_3 and HNO_3 diffusivities are affected by the presence of the organic film. That is, the diffusivity of NH_3 and HNO_3 through DOP is slow, thus resulting in low values of D_{eff} .

A rigorous interpretation of D_{eff} requires developing a new version of Eq. (6) which includes the DOP film. This would allow some estimation of the diffusion of NH_3 and HNO_3 through the DOP film. Also, the calculated values for D_{eff} are size dependent and should not be extrapolated to larger particle sizes and different film thicknesses than those presented in this study.

4.2. Implications to NH_4NO_3 equilibrium timescales

The observed reduction in NH_4NO_3 evaporation rate for particles larger than 150 nm due to an organic coating can affect the equilibration time for submicron atmospheric particles. Fig. 7 shows the predicted times for evaporation of NH_4NO_3 submicron particles, using the reduced values of $\alpha_{\text{NH}_4\text{NO}_3}$ which were observed in the DOP-coated experiments in Eqs. (6) and (7). The predicted times for evaporation indicate that for submicrometer particles, the equilibrium timescale is less than approximately 30 min at 22°C (Fig. 7). This represents a small increase from the calculations for pure NH_4NO_3 evaporation by Dassios and Pandis (1999), which predicted an equilibrium time of less than 17 min for the same particle size range. Likewise, the results at 27°C predict an evaporation time of less than 18 min for submicrometer organic-coated NH_4NO_3 particles, which represents only a 6 min increase in NH_4NO_3 equilibrium time over the pure particle, as predicted by Dassios and Pandis (1999). For particles less than 0.7 μm , the equilibration time remains under 20 min at 22°C, even with the

presence of the organic coating. Therefore, the equilibrium assumption for submicrometer particles appears to remain valid when considering the possibility of organic coatings similar to DOP.

5. Conclusions

A small decrease in NH_4NO_3 evaporation due to the presence of the DOP film was observed at 22 and 27°C. The decrease in evaporation due to the DOP can be parametrized by a decrease in the $\alpha_{\text{NH}_4\text{NO}_3}$ for pure NH_4NO_3 from 0.40 to 0.25 for the DOP-coated NH_4NO_3 at 22°C. Similarly, at 27°C, a decrease in $\alpha_{\text{NH}_4\text{NO}_3}$ from 0.30 for the pure experiment to 0.25 for the DOP-coated experiments is estimated. Assuming these values of $\alpha_{\text{NH}_4\text{NO}_3}$ for predicting evaporation times for DOP-coated NH_4NO_3 aerosol results in an increase in equilibration time of only a few minutes (e.g., from 17 min for a pure 1 μm NH_4NO_3 particle to 32 min for an organic-coated particles of the same size). Alternatively, the observed decrease in NH_4NO_3 evaporation can also be explained by an effective diffusivity, D_{eff} , which ranges, depending on particle size, from 0.01 to 0.1 $\text{cm}^2 \text{s}^{-1}$ for $T = 22^\circ\text{C}$ and from 0.03 to 0.07 $\text{cm}^2 \text{s}^{-1}$ for $T = 27^\circ\text{C}$. This is lower than the traditionally used diffusivities for NH_3 and HNO_3 in air (0.11 $\text{cm}^2 \text{s}^{-1}$). Both models indicate that the DOP could inhibit the mass transfer of NH_4NO_3 between the gas and aerosol phase, but the equilibration timescale for submicrometer NH_4NO_3 would still be of the order of minutes.

The results presented in this work are applicable to nearly dry NH_4NO_3 submicron aerosol coated with organics similar to DOP. Since DOP is a liquid organic which may form films over the core aerosol, other types of coatings, such as solid or porous coatings, may show a different effect on the evaporation rate of NH_4NO_3 . Also, our results are applicable for an organic film thickness of approximately 10–15 nm. Finally, the effect of water content must be further investigated as to determine the effect of organic coatings on the evaporation of deliquesced NH_4NO_3 particles, which would be relevant to high relative humidity atmospheric conditions.

Acknowledgements

This work was funded by the US Environmental Protection Agency (R-823514-01-0) and the Teresa Heinz Scholarship for Environmental Research (H0888).

References

Andrews, E., Larson, S., 1993. Effect of surfactant layers on the size changes of aerosol particles as a function of relative

- humidity. *Environmental Science and Technology* 27, 857–885.
- Ansari, A.S., Pandis, S.N., 1999. Prediction of multicomponent inorganic atmospheric aerosol behavior. *Atmospheric Environment* 33, 745–757.
- Bai, H., Lu, C., Ling, Y.M., 1995. A theoretical study on the evaporation of dry ammonium chloride and ammonium nitrate aerosols. *Atmospheric Environment* 29, 313–321.
- Basset, M.E., Seinfeld, J.H., 1984. Atmospheric equilibrium model of sulfate and nitrate aerosols. *Atmospheric Environment* 17, 2237–2252.
- Chow, J.C., Watson, J.G., Fujita, E.M., Lu, Z.Q., Lawson, D.R., Ashbaugh, L.L., 1994. Temporal and spatial variations of PM_{2.5} and PM₁₀ aerosol in Southern California air quality. *Atmospheric Environment* 28, 2061–2080.
- Cruz, C.N., Pandis, S.N., 1998. The effect of organic coatings on the cloud condensation nuclei activation of inorganic atmospheric aerosol. *Journal of Geophysical Research* 103, 13111–13123.
- Cruz, C.N., Pandis, S.N., 1999. Condensation of organic vapors on an externally mixed aerosol population. *Aerosol Science and Technology* 31, 392–407.
- Dassios, K.G., Pandis, S.N., 1999. The mass accommodation coefficient of ammonium nitrate aerosol. *Atmospheric Environment* 33, 2293–3003.
- Ellison, G.B., Tuck, A.F., Vaida, V., 1999. Atmospheric processing of organic aerosols in the marine boundary layer. *Journal of Geophysical Research* 104, 11633–11641.
- Fuchs, N.A., Sutugin, A.G., 1971. Highly dispersed aerosols. In: Hidy, G.M., Brock, J.R. (Eds.), *Topics in Current Aerosol Research, Part 2*. Pergamon, New York.
- Gill, P.S., Graedel, T.S., Weschler, C.J., 1983. Organic films on atmospheric aerosol particles, fog droplets, cloud droplets, raindrops, and snowflakes. *Reviews of Geophysics* 22, 903–920.
- Hameri, K., Rood, M.J., Hansson, H.C., 1992. Hygroscopic properties of a NaCl aerosol coated with organic compound. *Journal of Aerosol Science* 23, S437–S440.
- Hildemann, L.M., Russell, A.G., Cass, G.R., 1984. Ammonia and nitric acid concentrations in equilibrium with atmospheric aerosol: experiment vs. theory. *Atmospheric Environment* 18, 1737–1750.
- Liang, C., Pankow, J.F., Odum, J.R., Seinfeld, J.H., 1997. Gas/particle partitioning of semivolatile organic compounds to model inorganic, organic, and ambient smog aerosols. *Environmental Science and Technology* 31, 3088–3092.
- Mozurkewich, M., 1993. The dissociation constant of ammonium nitrate and its dependence on temperature, relative humidity, and particle size. *Atmospheric Environment* 27A, 261–270.
- Shulman, M.L., Charlson, R.J., Davis, E.J., 1997. The effects of atmospheric organics on aqueous droplet evaporation. *Journal of Aerosol Science* 28, 737–752.
- Sloane, C.S., Watson, J., Chow, J., Pritchett, L., Richards, L.W., 1991. Size-segregated fine particle measurements by chemical species and their impact on visibility impairment in Denver. *Atmospheric Environment* 25A, 1013–1024.
- Stelson, A.W., Seinfeld, J.H., 1982. Relative humidity and temperature dependence of the ammonium nitrate dissociation constant. *Atmospheric Environment* 16, 983–992.
- Tao, Y., McMurry, P.H., 1989. Vapor pressure and surface free energies of C₁₄–C₁₈ monocarboxylic acids and C₅ and C₆ dicarboxylic acids. *Environmental Science and Technology* 23, 1519–1523.
- Turpin, B.J., Huntzicker, J.J., 1991. Secondary formation of organic aerosol in the Los Angeles basin: a descriptive analysis of organic and elemental carbon concentrations. *Atmospheric Environment* 25A, 207–215.
- Turpin, B.J., Huntzicker, J.J., Larson, S.M., Cass, G.R., 1991. Los Angeles summer midday particle carbon: primary and secondary aerosol. *Environmental Science and Technology* 25, 1788–1793.
- Wexler, A.S., Seinfeld, J.H., 1990. The distribution of ammonium salts among a size and composition dispersed aerosol. *Atmospheric Environment* 24A, 1231–1246.
- Wexler, A.S., Seinfeld, J.H., 1992. Analysis of aerosol equilibrium ammonium nitrate: departures from equilibrium during SCAQS. *Atmospheric Environment* 26A, 579–591.
- Wolff, G.T., Ruthosky, M.S., Stroup, D.P., Korsog, P.E., 1991. A characterization of the principal PM-10 species in Claremont (summer) and Long Beach (fall) during SCAQS. *Atmospheric Environment* 25A, 2173–2186.
- Xiong, J.Q., Zhong, M., Fang, C., Chen, L.C., Lippmann, M., 1998. Influence of organic films on the hygroscopicity of ultrafine sulfuric acid aerosol. *Environmental Science and Technology* 32, 3536–3541.
- Ziemann, P.J., McMurry, P.H., 1998. Secondary electron yield measurements as a means for probing organic films on aerosol particles. *Aerosol Science and Technology* 28, 77–90.